# Nondestructive spatial heterodyne imaging of cold atoms

**S. Kadlecek, J. Sebby, R. Newell, and T. G. Walker**

*Department of Physics, University of Wisconsin–Madison, Madison, Wisconsin 53706*

Received August 31, 2000

We demonstrate a new method for nondestructive imaging of laser-cooled atoms. This spatial heterodyne technique forms a phase image by interfering a strong reference laser beam with a weak probe beam that passes through the cold atom cloud. The figure of merit equals or exceeds that of phase-contrast imaging, and the technique can be used over a wider range of spatial scales. We show images of a dark-spot magneto-optic trap taken with imaging fluences as low as 61 pJ/cm$^2$ at a detuning of 11$\Gamma$, resulting in 0.0004 photons scattered per atom. © 2001 Optical Society of America

*OCIS codes:* 110.0110, 020.7010, 120.5050.

In this Letter we demonstrate a new spatial heterodyne method for nondestructive imaging of trapped atoms. As with other nondestructive techniques, spatial heterodyne imaging minimizes the number of absorbed photons required for an image and is therefore particularly useful in applications such as Bose–Einstein condensation,[1–3] magnetic trapping, and far-off-resonance trapping that are particularly sensitive to heating and optical pumping from absorbed photons.

Off-resonant, nondestructive imaging of clouds of trapped atoms[4] was previously demonstrated with several different methods, all of which image the phase shift produced by the atoms on a collimated probe laser: dark-ground imaging,[5] polarization-rotation imaging,[6] and phase-contrast imaging.[7] Nondestructive detection without imaging was recently demonstrated by use of FM spectroscopy.[8] The most popular of these methods, the phase-contrast technique, uses a small (approximately 10 to 100 $\mu$m) $\pi/2$ phase mask that is inserted into the imaging laser focus at the Fourier plane of an imaging lens. In the image plane the $\pi/2$ phase-shifted laser field interferes with the signal field produced by the atoms to give an image intensity that is linear with respect to the atom-induced phase shift.

To implement spatial heterodyne imaging we used two laser beams: a reference laser beam, which does not pass through the trapped atoms, and a probe beam, which is phase shifted as it passes through the atom cloud. The beams interfere on a CCD camera, and we process the resulting interference pattern in software to reconstruct the phase shift that is due to the cloud.

Spatial heterodyne imaging has several practical advantages for nondestructive imaging. First, there is no need for precision fabrication and alignment of a phase plate. Second, this method has a significant signal-to-noise ratio (S/N) advantage for low imaging intensities. Third, at high intensities it has a larger signal per absorbed photon, thus making better use of the large dynamic range of CCD cameras. Fourth, the method works over a wide range of spatial scales. Finally, rejection of spurious interference fringes that are due to various optical elements is automatic.

The principle of spatial heterodyne imaging is similar to that of heterodyne spectroscopy,[9] with interference occurring in the spatial rather than the temporal domain. As shown in Fig. 1(a), a probe beam of intensity $I_p$ travels through a cloud of trapped atoms and accumulates a position-dependent phase shift $\phi(\mathbf{x})$, owing to the index of refraction of the atoms. A lens placed in this beam images the atom cloud onto a CCD detector. A reference beam of intensity $I_r$, derived from the same laser as the probe beam, interferes with the probe beam at angle $\theta$. For convenience, we assume equal radii of curvature for the reference and the probe beams. The interference pattern on the CCD detector, $I(\mathbf{x})$, is a set of straight line fringes whose position is determined by an overall phase shift between the beams $\chi$ and that is distorted by the accumulated phase shift from the atoms,

$$I(\mathbf{x}) = I_r + I_p + 2\sqrt{I_r I_p}\,\cos\left[\chi + 2\pi\theta\hat{k}_\perp \cdot \frac{\mathbf{x}}{\lambda} - \phi(\mathbf{x})\right], \quad (1)$$

from which $\phi(\mathbf{x})$ can be reconstructed. Here $\hat{k}_\perp$ is a unit vector pointing along the direction of the component of the reference wave vector $\mathbf{k}$ perpendicular to the direction of the probe beam.

Phase shift $\phi$ is most easily determined in two limits: $\theta \ll \delta/\lambda$ (parallel mode) and $\theta \gg \delta/\lambda$ (tilted mode), where $\delta$ is the desired resolution element on the image. In the parallel mode the phase of the interference pattern is uniform across the cloud image, and the resulting interference pattern is (with $\chi = \pi/2$)

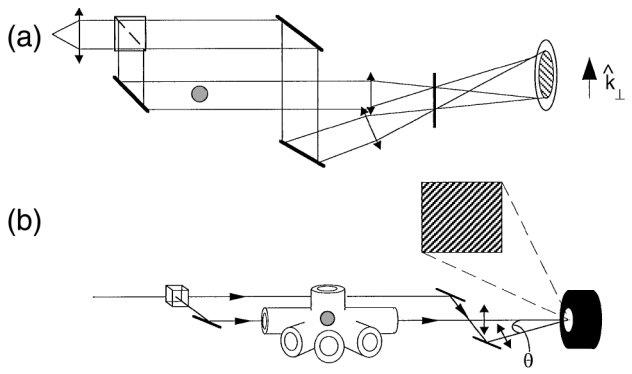


Fig. 1. Spatial heterodyne imaging apparatus. See text for details.

0146-9592/01/030137-03$15.00/0 

$$I(\mathbf{x}) = I_r + I_p + 2\sqrt{I_r I_p}\,\sin\,\phi(\mathbf{x}). \qquad (2)$$

If $I_r = I_p$, this pattern is identical to that of phase-contrast imaging. If not, the signal size is increased by a factor of $\sqrt{I_r/I_p}$. The spatial variation of the phase shift from the cloud becomes a spatial variation of the intensity at the CCD detector, producing a real image on the detector. In practice, phase shift $\chi$ must be stabilized by use of feedback.

For this Letter we have implemented spatial heterodyne imaging in the tilted mode. In this case, a set of high-spatial-frequency fringes appears, and the effect of the atom cloud is to give a spatially varying phase shift to these fringes. The analysis of the fringes then proceeds in a manner highly analogous to lock-in detection: We demodulate the interference pattern to zero spatial frequency and apply a low-pass filter to the result. Fast Fourier transform techniques make the demodulation and filtering efficiency (2 for a $784 \times 520$ pixel camera on a 400-MHz Pentium). It is not necessary to stabilize the relative phase between the probe and the reference beams.

To demonstrate the method we use an atom cloud with an on-resonant optical thickness of $\sim$15 in a dark-spot $^{87}$Rb magneto-optic trap (MOT).[10,11] The experimental arrangement is shown in Fig. 1(b). Typically $3 \times 10^7$ atoms from a MOT are accumulated in the dark state at a density of roughly $5 \times 10^{11}$ cm$^{-3}$ by imaging of a 1-mm obstruction in the MOT repumping laser onto the trap. The atoms in the dark spot are quite sensitive to resonant light, and hence absorption imaging is difficult. The imaging laser beam is tuned to the range $2-11\Gamma$ from the $^{87}$Rb $5S_{1/2}(F = 1) \rightarrow 5P_{1/2}(F = 2)$ resonance, switched via an acousto-optic modulator, and then split into two beams by a nonpolarizing beam splitter. The probe beam is attenuated by a factor of 1–200 by a neutral-density filter before passing through the atom cloud, which is imaged onto a CCD array. An interference filter placed in the Fourier plane of the imaging lens rejects 780-nm fluorescence from the bright-state trapped atoms. The reference passes around the vacuum chamber and is incident upon the CCD detector tilted at an angle $\theta \approx 1°$. For convenience, we roughly match the radii of curvature of the probe and the reference beams at the CCD to produce nearly straight fringes. We tilt the fringes at an angle of typically 30° from the rows of the CCD chip to avoid aliasing.

Two competing factors determine the optimum angle $\theta$. As with lock-in detection, it is important to modulate the signal at a spatial frequency somewhat higher than the smallest feature to be resolved. The finite camera pixel size sets an upper limit on the modulation frequency without loss of fringe contrast. We find that a fringe spacing of 4–5 pixels is a good compromise between resolution and fringe contrast. In the parallel mode, full resolution of the camera is achieved.

To begin processing we subtract reference images of each laser beam. This leaves only the interference term in Eq. (1), which we Fourier transform. The transform contains the phase-image information in two sections centered on spatial wave numbers, $k_0 = \pm 2\pi\theta/\lambda$. We shift one of these sections to zero spatial frequency and attenuate the high frequencies with a filter, typically the Gaussian filter $\exp[-(3k/k_0)^2]$. Finally, we take the inverse transform whose phase $[\tan^{-1}(\mathrm{Im}/\mathrm{Re})]$ is $\phi(\mathbf{x})$. This procedure automatically reduces spurious interference fringes that arise from various optical elements, since they are likely to be at the wrong spatial frequency. To compensate for slight curvature of the interference fringes we subtract $\phi(\mathbf{x})$ from another image, similarly processed but taken in the absence of atoms. This compensation also reduces distortion owing to spatial inhomogeneities in $I_r$ and $I_p$.

Figure 2 shows several images of $\phi(\mathbf{x})$ taken by use of the above procedure. At a typical line center optical thickness of 3–15 we successfully imaged the dark-spot trap for a variety of detunings and reference-to-probe intensity ratios $R$. Figure 2(a) shows a typical image with $R = 20$, $\Delta = -11\Gamma$, and $\sim 1.2 \times 10^{-3}$ scattered photons per atom. As another example, Fig. 2(b) shows an image taken at $\Delta = -11\Gamma$ and $R = 60$. The total fluence used to make the image was only 61 pJ/cm$^2$, corresponding to 0.0004 photons scattered per atom. The S/N of a given resolution element is $\sim$10 for this image.

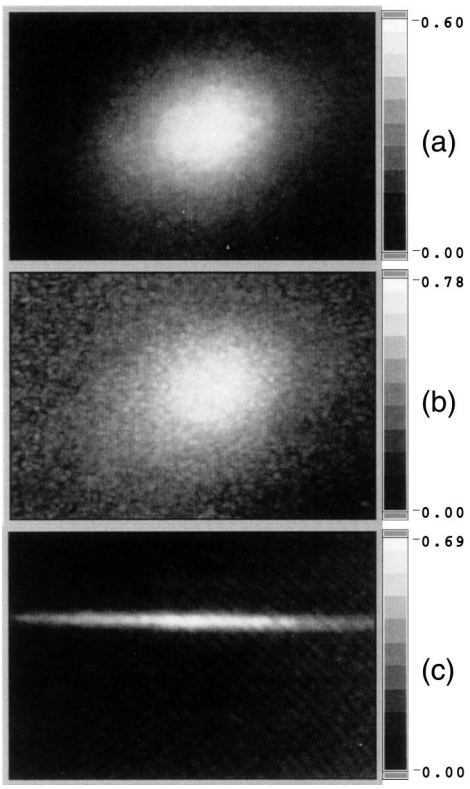


Fig. 2. (a) Image of a dark-spot MOT taken at a probe detuning $\Delta = -11\Gamma$ and reference-to-probe intensity ratio $R = 20$. (b) Image optimized for minimum light scattering: $\Delta = -11\Gamma$, $R = 60$. Obtaining this image required that approximately 0.0004 photons be scattered per atom. (c) Side-on image of a dark-sheet trap formed by a 59-$\mu$m wire image in the repumping beam. The image of the cloud is approximately 51 $\mu$m. The right-hand scale is the phase shift in radians.

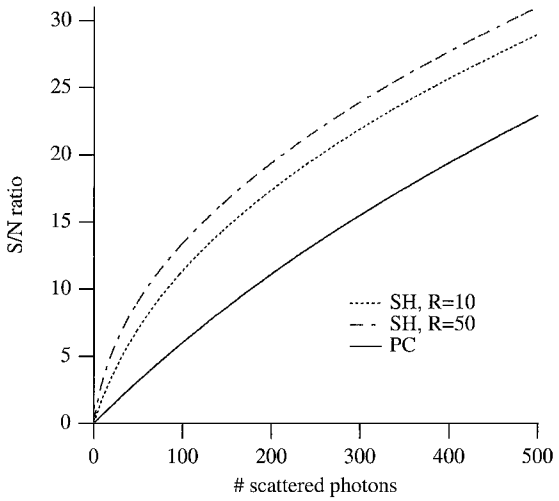


Fig. 3. S/N comparison for phase-contrast (PC) imaging and spatial heterodyne (SH) imaging for two reference-to-probe intensity ratios $R$. The camera's read noise is assumed to be $b = 25$ e$^-$, and the quantum efficiency is $\eta = 0.5$.

Depending on the details of the imaging system, filtering of the Fourier transform may limit the spatial resolution of the final image. In our system, with a magnification of 5 and a CCD pixel spacing of 8.8 $\mu$m, the resolution is limited to $\sim$20 $\mu$m, compared with a theoretical diffraction limit of $\sim$5 $\mu$m. Figure 2(c) shows an image of a 50-$\mu$m-wide trap.

Depending on the application, the figure of merit for spatial heterodyne imaging is comparable with or superior to phase-contrast imaging. For simplicity, we consider here the parallel mode. The number of photons striking a given image pixel is $N_r + N_p + 2\sqrt{N_r N_p}\,\cos[\chi - \phi(x)]$. For small phase shifts and $\chi \approx \pi/2$, the signal size is approximately $2\eta\sqrt{N_r N_p}\,\phi$, where $\eta$ is the quantum efficiency of the detector, typically $\sim$0.3 for CCD chips in the near infrared. Noise sources include shot noise and other sources of technical noise, $b$, such as the camera's read noise and the finite resolution of the camera's analog–digital converter. The S/N is therefore

$$(\mathrm{S/N})_{\mathrm{SH}} = \frac{2\eta\phi\sqrt{N_r N_p}}{[\eta(N_r + N_p) + b^2]^{1/2}}. \tag{3}$$

The maximum S/N occurs for $N_r \gg N_p,\ b^2/\eta$, giving

$$(\mathrm{S/N})_{\mathrm{max}} = 2\phi\sqrt{\eta N_p}, \tag{4}$$

which shows that there is a minimum number of photons that must be scattered from the atoms for a given S/N. A similar relation holds for phase-contrast imaging.

A natural figure of merit for nondestructive imaging is the number of absorbed photons $A$ required for the desired S/N. For optically thick clouds this number is greatly reduced because the probing can be done at large detuning.[4] Thus the shot-noise-limited figure of merit for either technique is

$$\frac{\mathrm{S/N}}{A} = \frac{2\phi\sqrt{\eta N_p}}{\alpha N_p} \approx \frac{2\Delta}{\Gamma}\sqrt{\frac{\eta}{N_p}} \tag{5}$$

for $\Delta \gg \Gamma$. Here we use $\phi/\alpha \approx \Delta/\Gamma$ to relate absorption coefficient $\alpha$ to $\phi$.

When the technical noise, $b$, is significant, however, spatial heterodyne imaging has a better S/N raio than phase-contrast imaging. Figure 3 shows a comparison of the S/N's ratios of the two techniques as a function of the number of scattered photons. As with any heterodyne method, the interference between the reference and the signal boosts the signal level at a given probe intensity.

Furthermore, for highest image quality it is desirable to maximize signal size and thereby minimize the discretization errors from the analog–digital converter. In this case the spatial heterodyne method offers a $\sqrt{R}$ performance enhancement compared with the phase-contrast technique. Figure 2(b) shows an image taken with $R = 60$, representing 3 bits of increased signal size for fixed absorption.

We have demonstrated the spatial heterodyne method for nondestructive imaging of trapped atoms and shown that it has advantages over other techniques. Our method is a special case of a more general class of holographic imaging techniques that could be used.

Support for this research came from the National Science Foundation. We acknowledge helpful communications with D. Jin, W. Ketterle, and S. Rolston and technical assistance from N. Harrison. J. Sebby's e-mail address is jssebby@students.wis.edu.

## References

1. M. Anderson, J. Ensher, M. Matthews, C. Wieman, and E. Cornell, Science **269,** 198 (1995).
2. K. Davis, M.-O. Mewes, M. R. Andrews, N. J. van Druten, D. S. Dufree, D. M. Kurn, and W. Ketterle, Phys. Rev. Lett. **75,** 3969 (1995).
3. C. Bradley, C. Sackett, and R. Hulet, Phys. Rev. Lett. **78,** 985 (1997).
4. W. Ketterle, D. S. Durfee, and D. M. Stamper-Kurn, in *Bose–Einstein Condensation in Atomic Gases*, M. Inguscio, S. Stringari, and C. E. Wieman, eds., Vol. 140 of Proceedings of the International School of Physics Enrico Fermi (IOS Press, Amsterdam, 1999), pp. 67–176.
5. M. R. Andrews, M.-O. Mewes, N. J. van Druten, D. S. Durfee, D. M. Kurn, and W. Ketterle, Science **273,** 84 (1996).
6. C. C. Bradley, C. A. Sackett, and R. G. Hulet, Phys. Rev. Lett. **79,** 985 (1997).
7. M. R. Andrews, D. M. Kurn, H.-J. Miesner, D. S. Durfee, C. G. Townsend, S. Inouye, and W. Ketterle, Phys. Rev. Lett. **79,** 553 (1997).
8. V. Savalli, G. Horvath, P. Featonby, L. Cognet, N. Westbrook, and C. Westbrook, Opt. Lett. **24,** 1552 (1999).
9. A. Yariv, *Optical Electronics*, 2nd ed. (Holt, Rinehart & Winston, New York, 1976).
10. W. Ketterle, K. B. Davis, M. A. Joffe, A. Martin, and D. E. Pritchard, Phys. Rev. Lett. **70,** 2253 (1993).
11. M. H. Anderson, W. Petrich, J. R. Ensher, and E. A. Cornell, Phys. Rev. A **50,** R3597 (1994).